Effects of Contact Geometry on Pull-Off Force Measurements with a Colloidal Probe

Seungho Yang,† Huan Zhang,*,†,‡ Michael Nosonovsky,† and Koo-Hyun Chung†

National Institute of Standards and Technology, 100 Bureau Drive, Gaithersburg, Maryland 20899, and Institute for Physical Science and Technology, University of Maryland, College Park, Maryland 20742

Received June 26, 2007. In Final Form: October 24, 2007

This paper examines the effects of contact geometry on the pull-off (adhesion) force between a glass sphere (colloidal probe) and a silicon wafer in an environment with controlled relative humidity. An atomic force microscope is used to measure the pull-off force between the colloidal probe and the sample mounted at different tilt angles. The results show that the measured pull-off force is very sensitive to the tilt angle. Through the use of a newly developed direct scanning method, the exact contact geometry is determined for the zero-tilt angle case. The obtained digital image is then rotated to determine the contact geometry for the cases with other tilt angles. A detailed examination of the contact geometry, along with a magnitude analysis of the capillary force, suggests that the adhesion is most likely dominated by the capillary force from the meniscus formed between the probe and the sample. The strong dependence of the adhesion on the tilt angle may result from the change of meniscus dimensions associated with the probe−sample separation, which in turn is controlled by the highest peak on the probe sphere. Our observation emphasizes the combined role of microsurface shape near the contact and nanoroughness within the contact in determining the colloidal probe pull-off force and also microadhesion force in general.

1. Introduction

Adhesion is a general term for the attractive forces acting between surfaces, such as capillary forces, van der Waals forces, chemical bonding forces, and electrostatic forces. At the microscale and below, devices and particles are highly susceptible to these surface forces because of their extremely high surface-to-volume ratio. Consequently, adhesion is one of the key mechanisms that determine the interaction between components in microelectomechanical systems (MEMS) and microfluidic devices. For example, strong adhesion may cause stiction in fabrication and operation, leading to production loss and triggering catastrophic failures.[1,2] In addition, extremely high-density magnetic storage recording requires ultralow flying super smooth head-disk interfaces (HDI).[3] Strong adhesion and friction may be present under these conditions, causing premature HDI failure. For dry powder inhalers (DPIs), which deliver proteins or other macromolecules to the lungs, therapeutic agents are stored as their own aggregates or bonded to stabilizing carriers. In either form, the powder mixture must be dispersed into inhalable aerosols by using certain means of energy to overcome the adhesion forces between the drug particles themselves or between the particles and the carriers.[4] Therefore, accurate characterization of micro- and nanoscale adhesion forces is a prerequisite for further development of microdevices and next-generation magnetic storage recording and drug delivery systems.

Many theoretical models are available to relate the solid-to-solid adhesion to material properties such as surface energy for simple contact geometry. The Johnson−Kendall−Roberts (JKR) model accounts for the influence of van der Waals forces within the contact zone for the sphere-to-plane contact with large radius and low stiffness.[5] For the same geometric configuration but with small radius and large stiffness, the Derjagin−Muller−Toropov (DMT) model considers van der Waals forces acting in the vicinity of the contact area.[6] These two models suggest a similar linear dependence of the pull-off force on the sphere radius and surface energy, which is needed to separate the surfaces in the normal direction and is commonly used to characterize adhesion.

In an environment containing a condensable vapor, a curved meniscus is usually formed by the condensation of liquid between two close solid surfaces. A pressure drop across the meniscus gives rise to the capillary force which dominates the adhesion as the van der Waals attraction is much reduced in this case.[7] For the sphere−plane contact, the capillary force is also a linear function of the sphere radius as derived by using the Laplace equation which relates the pressure drop to the meniscus dimensions.[8]

The linear relation between the pull-off force and the surface radius of curvature has been verified experimentally in the case of smooth surfaces with radii of curvature down to the millimeter and sub-millimeter range.[9−11] Accordingly, the pull-off force measurement has been used to determine the surface energy.

The invention of the atomic force microscope made it possible to study nano- and microscale adhesion by measuring the pull-off force between an atomic force microscope (AFM) tip and a

* To whom correspondence should be addressed. E-mail: huan.zhang@nist.gov. Telephone: 301-975-2917. Fax: 301-975-5334.

† National Institute of Standards and Technology.

‡ University of Maryland.

(1) Mastrangelo, C. H.; Hsu, C. H. *IEEE J. Microelectromech. Syst.* **1993**, *2*, 33−43.

(2) Walraven, J. A. *ITC Int. Test Conf.* **2003**, 828−833.

(3) Wood, R. W.; Miles, J.; Olson, T. *IEEE Trans. Magn.* **2002**, *38*, 1711−1718.

(4) Iida, K.; Hayakawa, Y.; Okamoto, H.; Danjo, K.; Leuenberger, H. *Chem. Pharm. Bull.* (*Tokyo*) **2003**, *51*, 1−5.

(5) Johnson, K. L.; Kendall, K.; Roberts, A. D. *Proc. R. Soc. London, Ser. A* **1971**, *324*, 301−313.

(6) Derjaguin, B. V.; Muller, V. M.; Toporov, Y. P. *J. Colloid Interface Sci.* **1975**, *67*, 314−326.

(7) Wan, K. T.; Smith, D. T.; Lawn, B. R. *J. Am. Ceram. Soc.* **1992**, *75*, 667−676.

(8) Israelachvili, J. N. *Intermolecular and Surface Forces*, 2nd ed.; Academic Press: London, 1992.

(9) Fuller, K. N. G.; Tabor, D. *Proc. R. Soc. London, Ser. A* **1975**, *345*, 327−342.

(10) Horn, R. G.; Israelachvili, J. N.; Pribac, F. *J. Colloid Interface Sci.* **1987**, *115*, 480−492.

(11) McFarlane, J. S.; Tabor, D. *Proc. R. Soc. London, Ser. A* **1950**, *202*, 224−243.

10.1021/la701900f Published 2008 by the American Chemical Society
Published on Web 01/03/2008

sample surface. However, it is difficult to use the abovementioned models to interpret the experimental results and then extract the surface energy because of the complex tip geometry. The "colloidal-probe" technique has been introduced to ease the complexity by attaching a spherical microparticle to the end of an AFM cantilever.[12,13] The theories based on the spherical contact geometry are then expected to be valid. Subsequently, the pull-off forces measured with the technique could be normalized by the probe radius to characterize the surface energy with reasonable reproducibility. However, these measurements usually show poor reproducibility.[14−16]

Efforts have been made to understand and resolve the lack of reproducibility to realize the full potential of the colloidal-probe technique in adhesion characterization.[17−22] These studies suggested that the major causes for the scatter (irreproducibility) in the measurements could be roughness and heterogeneity of the probe surface and the sample. Thus, determination of the precise contact position and the corresponding topographic information is extremely important to understand this phenomenon. Rabinovich et al.[20,21] proposed a model to account for the effects of nanoscale roughness on the adhesion due to van der Waals forces in terms of the maximum peak height. The model determined this parameter based on its relation with the root-mean-square (rms) value instead of using the height of the real highest peak. Farshchi-Tabrizi et al.[22] calculated the meniscus force with a two-sphere model to take into account different AFM tip (or particle) shapes. More recently, Yang et al.[23] measured pull-off forces for colloidal probes of different radii in dry air (relative humidity (RH) < 3%). They then successfully correlated the measurement to the specific contact geometry by finding the exact contact spot with a direct scanning method developed from the reverse AFM imaging approach.[24]

This paper focuses on how the topography of the precise contact zone affects the adhesion that is dominated by the capillary forces. First, we measured the pull-off force between a single probe and a silicon wafer sample mounted on wedges of different angles under controlled relative humidity. The topography of the actual contact spot was then obtained for the case of zero tilt with the direct scanning method.[23] The real contact shifts to a different spot on the colloidal probe when the sample is tilted. Next, the topography of the new contact spot was determined by using a digital rotation of the measured AFM image. By examining in detail the topography of the contact spot at each angle, we gained insights into the effects of the precise contact geometry on adhesion under relatively humid conditions.

2. Experimental Procedure

2.1. Sample Preparation. A colloidal probe was prepared by gluing (Loctite, QuickSet[th] Epoxy[25]) a glass sphere (NIST, SRM 1003C[25]) on a silicon cantilever (Veeco, ULCT-AUNM[25]). Figure 1 shows a scanning electron microscopic image of the probe. We scanned a silicon grating sample (TGT 01, NT-MDT[25]) with the colloidal probe and determined the nominal radius of the probe to be 10 ± 0.5 μm. After the scanning, the colloidal probe was plasma-cleaned (Harrick Plasma Cleaner, PDC-001[25]) for 30 s to eliminate possible contamination from the grating sample. In addition, silicon wafer (100) (Polishing Corporation of America[25]) samples were cleaned in an ultrasonic bath with high purity ethanol for 1 min and then in the plasma cleaner for 30 s before use. The cleaning process removed organic and inorganic deposits on the sample and the surface of the colloidal probe so as to reduce the uncertainty of force measurement associated with the unknown mechanical and chemical properties of the deposits.

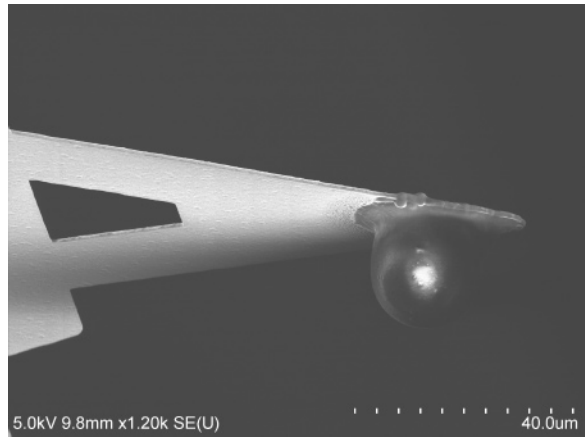

Figure 1. SEM image of the colloidal probe attached to an AFM cantilever.

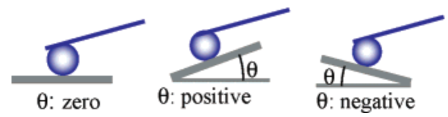

Figure 2. Colloidal probe in contact with silicon samples mounted on wedges at different tilt angles.

Finally, we note that the spring constant of the cantilever must always be calibrated before the pull-off force is measured with the AFM. For the probe cantilever used in this work, calibration with a reference cantilever (Veeco, CLFC-NOBO[25]) showed that it had a spring constant of 4.1 ± 0.6 nN/nm.

2.2. Pull-Off Force Measurement. The pull-off force between the cleaned colloidal probe and silicon (100) wafer samples was measured by using an AFM (Veeco, Multimode IIIa[25]) in a vibration-free, temperature-controlled clean environment. To demonstrate the effects of probe roughness on adhesion, the cleaned silicon (100) samples were mounted on five wedges with different tilt angles. As illustrated in Figure 2, each of these wedges can be arranged in two different configurations: one with a positive tilt angle (counter-clockwise) and the other with a negative tilt angle (clockwise). Including the case of zero tilt, the pull-off forces were measured and the corresponding topography was examined at a total of 11 tilt angles ranging from −5.7° to 5.7°. Moreover, the measurements were made at a constant room temperature of 20 ± 0.1 °C and at a relative humidity of 68% which was monitored with a digital hygrometer (Oakton, 35612, Thermo hygrometer[25]). For each tilt angle, a minimum of six pull-off tests were conducted at different locations of the wafer to reduce the statistical uncertainty.

2.3. Direct Method for Measuring the Topography of the Actual Contact Spot. An interpretation of the pull-off force

(12) Butt, H. J. *Biophys. J.* **1991**, *60*, 1438−1444.
(13) Ducker, W. A.; Senden, T. J.; Pashley, R. M. *Nature* (*London*) **1991**, *353* (6341), 239−241.
(14) Drelich, J.; Tormoen, G. W.; Beach, E. R. *J. Colloid Interface Sci.* **2004**, *280*, 484−497.
(15) Mittal, K., Ed. *Contact Angle, Wettability and Adhesion*; VSP: Leiden-Boston, 2004; Vol. 4.
(16) Drelich, J.; Mittal, K. L. *Atomic Force Microscopy in Adhesion Studies*; VSP: Utrecht-Boston, 2005.
(17) Heim, L.-O.; Ecke, S.; Preuss, M.; Butt, H.-J. *J. Adhes. Sci. Technol.* **2002**, *16*, 829−843.
(18) Heim, L.-O.; Blum, J. *Phys. Rev. Lett.* **1999**, *83*, 3328−3331.
(19) Heim, L.-O.; Kappl, M.; Butt, H.-J. *Langmuir* **2004**, *20*, 2760−2764.
(20) Rabinovich, Y. I.; Adler, J. J.; Ata, A.; Singh, R. K.; Moudgil, B. M. *J. Colloid Interface Sci.* **2000**, *232*, 10−16.
(21) Rabinovich, Y. I.; Adler, J. J.; Ata, A.; Moudgil, B. M. *J. Colloid Interface Sci.* **2000**, *232*, 17−24.
(22) Farshchi-Tabrizi, M.; Kappl, M.; Cheng, Y.-J.; Gutmann, J.; Butt, H.-J. *Langmuir* **2006**, *22*, 2171−2184.
(23) Yang, S. H.; Zhang, H.; Hsu, S. M. *Langmuir* **2007**, *23*, 1195−1202.
(24) Neto, C.; Craig, V. S. J. *Langmuir* **2001**, *17*, 2097−2099.
(25) Certain instruments and materials are identified to adequately specify the experimental procedure. Such identification does not imply recommendation or endorsement by the National Institute of Standards and Technology, nor does it imply that the materials or instruments identified are necessarily the best available for the purpose.

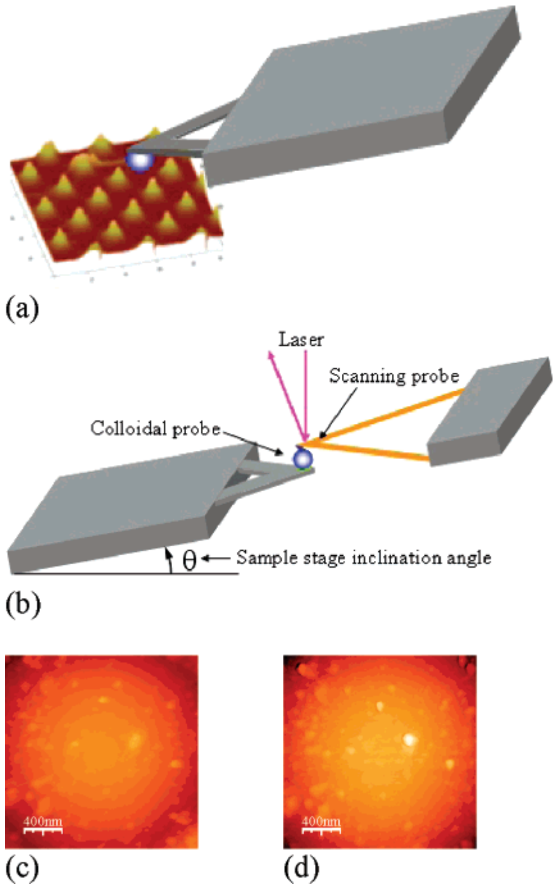

Figure 3. Schematic illustrations of the (a) reverse and (b) direct scanning methods of measurement of the surface topography with an AFM. Images of the colloidal probe obtained with (c) the reverse scanning method and (d) the direct scanning method.

measurements requires acquiring and characterizing the topography of the contact spots at each tilt angle in great detail and accuracy. To the authors' knowledge, there was no published method for this excluding the reverse AFM imaging method suggested by Neto and Craig, which could provide only low-quality topography.[24] To obtain a high-resolution and low-noise topographic image of the contact spot, a direct method has been applied successfully to study the roughness effects on adhesion in dry air.[23] This exact method is explained here in detail.

As illustrated in Figure 3a and b, the proposed method locates the exact contact spot on the colloidal probe and acquires a high-resolution topography of the probe around this spot in two steps. First, the colloidal probe is used to scan a grating sample (TGT1, NT-MDT[25]). The scanning produces a reverse image of the colloidal probe tip rather than an image of the grating sample, since the probe is much larger than the grating spikes. Second, the mirror image serves as a reference for the images generated by scanning the colloidal probe tip with a very compliant cantilever equipped with a fresh sharp tip, as shown in Figure 3b. For the current study, an oxide-sharpened silicon nitride tip was used. During scanning, the colloidal probe is mounted on sample wedges with different inclination angles. By adjusting the inclination angle, the topography of the actual contact spot is obtained when the position of an easily identifiable feature on the surface matches exactly with its position in the reference image.

Using the method described above, we measured the topography of the probe tip around the exact contact spot for the case in which the sample was not tilted. Figure 3c and d shows the images produced by the reverse scanning method and obtained by our direct method. In comparison, the direct method provides a much superior image that is characterized by clearer and readable features and less noise. The following two factors contribute to the high quality of the direct scanning method in topography measurement. First, this method

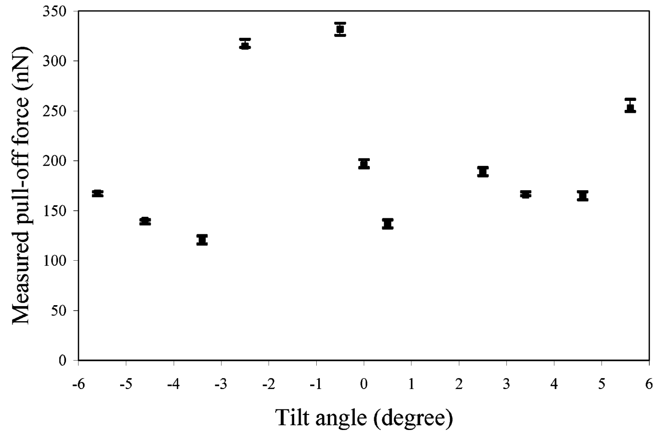

Figure 4. Measured pull-off force vs wedge tilt angle. The result is highly sensitive to small changes of the tilt angle due to the effect of the colloidal probe roughness. A small change in the tilt angle causes a significant change in the pull-off force.

uses a cantilever that is much more compliant than the one in the colloidal probe. The higher compliance results in a higher z-resolution image. Second, the unavoidable irregularity in spike shapes of the grating sample also affects the quality of the reverse scanning method.

When the sample was tilted a certain angle, the contact occurs at a different spot on the colloidal probe. In this situation, the topography of the new contact spot was produced by rotating the zero-tilt digital image. The procedure of rotation and the analysis of topography will be discussed later in the paper.

3. Experimental Results and Analysis

Figure 4 presents the measured pull-off forces for the 11 tilt angles. For each of these angles, multiple (6−10 times) pull-off force measurements were obtained at different locations of the wafer and their maximum, mean, and minimum values are illustrated in the figure. The results show that the repeated measurements at each tilt angle are highly reproducible and vary within ±5% from their respective averages. In contrast to the high reproducibility of the measurements for the same tilt angle, the average pull-off force changed dramatically when the sample was slightly tilted. For example, the average value of the measured pull-off force increased by 140% when the tilt angle was changed from +0.5° to −0.5°. Moreover, a one-way analysis of the variance of the data produced a zero *p*-value also indicating that there is no statistical correlation between the averages at different tilt angles.[26] In other words, no obvious trend is shown in Figure 4 although the pull-off force is sensitive to the change of the tilt angle of the sample surface.

A 3D numerical model predicts that the capillary force between a conical tip and a plane increases with increasing tilt angle, regardless of the direction of tilting.[27] According to this model, the dependence of the capillary force on the tilt angle results from the change of the meniscus caused by the tilting. In addition, the more similar the tip is to a sphere, the less the dependence. For the colloidal probe studied in this work, in spite of its normal spherical shape, the measured pull-off force is very drastically sensitive to the tilt angle. This sensitivity may be related to the dependence of the size and shape of the meniscus on the nanoscale roughness of the colloidal probe in the actual contact zone, as the capillary force is the major component of the pull-off force. To further clarify the underlying mechanisms of the phenomenon,

(26) Hogg, R. V.; Ledolter, J. *Engineering Statistics*; MacMillan: New York, 1987.
(27) Chau, A.; Rignier, S.; Delchambre, A.; Lambert, P. *Modell. Simul. Mater. Sci. Eng.* **2007**, *15*, 305−317.

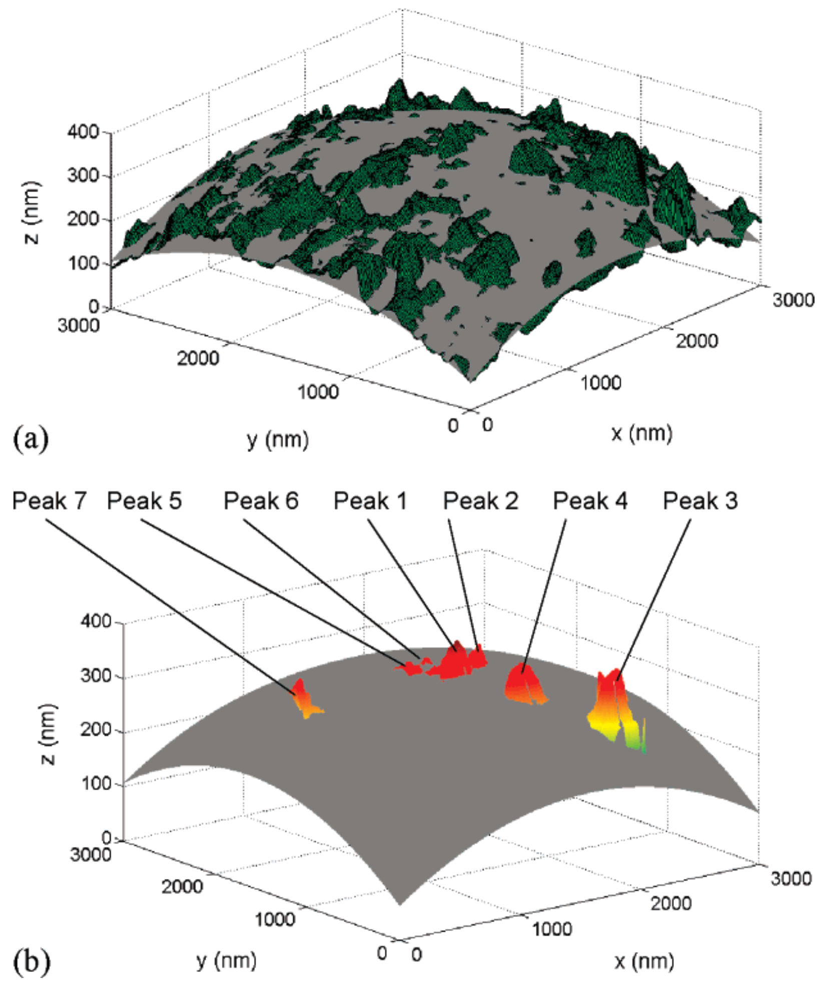

Figure 5. For the zero-tilt angle case: (a) measured topography of the colloid probe with its spherical shape determined from nonlinear least-square fitting and (b) the seven highest peaks on the probe surface.

we examined the topography of the contact spot determined with the direct scanning method and its change with the tilt angle.

Figure 5a presents the measured topography of the probe tip superimposed with the nominal spherical shape of the probe obtained as the result of nonlinear least-square fitting of the topography. The fitting determines the nominal radius R_{cp} of the probe and its center coordinates x_c, y_c, and z_c by solving the following minimization problem:

$$\min_{(R_{cp}x_c y_c, z_c)} \left(\sum_{i=1}^{N}\{z_i - [z_c + \sqrt{R_{cp}^{\ 2} - (x_i - x_c)^2 - (y_i - y_c)^2}]\}^2\right) \tag{1}$$

where N is the number of points on the surface selected for performing the fitting operation and x_i, y_i, and z_i ($i = 1, 2, ..., N$) are their coordinates. These points are equally spaced in the x-y plane. With the topography obtained from the direct scanning for the zero-tilt angle case, the fitting or minimization problem defined by eq 1 is solved and the resulting fitted sphere is shown in Figure 5a. This figure illustrates that the topography of the probe is characterized by multiple peaks above the fitted sphere surface. The number of the peaks in the contact zone and their heights and sizes (radii of curvature) may control the meniscus or menisci formed between the probe and the sample. In addition, the formation of menisci also depends on the level of relative humidity. It is plausible that the pull-off force between the probe and the sample mainly comes from separate nanoscale menisci formed at distributed highest peaks across the contact zone.

Table 1. Heights and Radii of Curvature of the Seven Highest Peaks on the Probe Surface When There Is No Tilt

peaks	height (nm)	radius of curvature (nm)
1	391.5	21.9
2	369.4	27.4
3	368.0	30.2
4	367.7	35.7
5	352.1	68.6
6	351.8	76.8
7	350.9	60.3

Figure 5b shows the highest seven peaks on the probe surface for the no-tilt case. These peaks are identified by using the watershed transform of the reversed topography of the probe.[28] For the probe tip topography, a single peak can thus be specified as a watershed or adjoining watersheds of its reverse image. For the peaks shown in Figure 5b, Table 1 lists their heights and approximate radii of curvature estimated as

$$r_c \approx A_{c-s}(\delta)/2\pi\delta \tag{2}$$

where r_c is the radius of curvature of a peak and $A_{c-s}(\delta)$ is its cross-sectional area at a given depth δ. Equation 2 provides a reasonable approximation for r_c with $\delta \ll r_c$. The depths used

(28) Luc, V.; Soille, P. *IEEE Trans. Pattern Anal. Mach. Intell.* **1991**, *13*, 583−598.

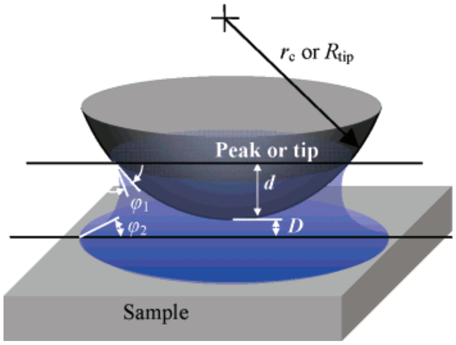

Figure 6. Schematic of a sphere−plate contact in the presence of a meniscus.

to estimate r_c are between 1 to 2 nm. If a meniscus is formed between a single peak and the sample, as illustrated in Figure 6, the resulting capillary force is then given by[8]

$$F_{cp} = \frac{4\pi r_c \gamma_L \cos\varphi}{(1 + D/d)} \tag{3}$$

where γ_L is the surface tension of liquid water, φ is the water contact angle with the surfaces, D is the peak−sample separation, and d is the depth of the peak immersed in the meniscus. In deriving eq 3, it was assumed that the contact angles with the two materials shown in Figure 6 are basically the same, that is, $\varphi_1 \approx \varphi_2$. The assumption is valid for this study, since the contact angle for a glass sphere with a diameter of less than 50 μm is approximately 25°,[29] whereas with a silicon wafer it is approximately 31°.[30] Equation 3 is therefore used next to calculate the approximate maximum capillary force from a meniscus by taking the separation D as zero and the values of the two contact angles to be 30°.

For the current study, $\gamma_L = 0.0729$ N m^{-1}. The maximum capillary force from the highest peak (peak 1 in Table 1) is about 20 nN, which is much smaller than the measured pull-off force of about 195.6 nN. Table 1 shows that peak 1 is at least 20 nm higher than any other peak on the surface. Thus, this peak needs to be significantly compressed before the menisci at lower peaks could provide a significant contribution to the total pull-off force. However, the compression of the peak may lead to a large resistance force, which can be estimated based on the Hertzian contact solution[31] as

$$F_r(\delta) = \frac{4E^*}{3}(r_c\delta)^{1/2}\delta \tag{4}$$

where δ represents the local compression and $E^* = ((1 - \upsilon_1^2)/E_1 + (1 - \upsilon_2^2)/E_2)^{-1}$ in which υ is the Poisson ratio, E is the material elastic modulus, and the subscripts refer to the probe (1) and the sample (2). With a small compression of $\delta = 2$ nm, the resistance force estimated from eq 4 is as high as 721.9 nN. This force would be much higher than meniscus forces from peaks other than the highest one, which can also be approximately estimated by using eq 3. Thus, the increase of capillary forces due to the decrease of separation could not compensate the increase of resistance force caused by the peak compression. This implies that, in the current experimental setting, it seems unlikely that multiple menisci would form between the sample and discrete peaks on the probe surface. The more likely scenario here is that a single, continuous meniscus forms between the probe and the sample, as illustrated in Figure 6.

Considering the possible resistance to the compression of individual peaks as discussed above, the highest peak on the probe largely determines the separation between its nominal spherical shape and the wafer. This separation D can be approximated by the maximum height of the real probe surface above the highest point of the nominal sphere surface. This maximum height, denoted as h_{m-s}, is defined as

$$h_{m-s} = z_{max} - z_c - R_{cp} \tag{5}$$

where z_{max} is the maximum z-coordinate of the probe surface. As the sample is tilted, the value of h_{m-s} changes, leading to the change of the separation and pull-off force. Based on this understanding, we can calculate the specific maximum heights for all the tilt angles tested and examine their correlation with the corresponding measured pull-off force.

In the absence of any tilt as was explained earlier, the nonlinear least-square fitting of the measured topography to a sphere provided the radius and center coordinates of the nominal sphere of the probe. With these results, the value of h_{m-s} can be calculated from eq 5. When the tilt angle is changed, the position and height of the highest peak on the probe changes or a different peak may become the highest one. Since tilting the sample is equivalent to the rotation of the probe, these changes are determined for each nonzero-tilt angle by digital rotation of the measured topography profile. The examination of the mounting of the sample and the AFM image of the probe indicates that the sample rotation illustrated in Figure 2 corresponds to the rotation of the 3D digital probe topography around the x-axis. After rotation by an angle θ, the new position (x', y', z') of a point (x, y, z) in the original coordination system is defined by

$$x' = x \tag{6a}$$

$$y' = y_c + (y - y_c)\cos\theta - (z - z_c)\sin\theta \tag{6b}$$

$$z' = z_c + (y - y_c)\sin\theta + (z - z_c)\cos\theta \tag{6c}$$

With all three parts of eq 6, the topography around the contact spot is obtained for each tilt angle and the corresponding maximum peak height h_{m-s} is then determined. The digital image rotation allows us to avoid the possible inclination-induced image distortion in the direct topography measurement with the atom force microscope.[32] In addition, for small tilt angles, we can assume that the peak points at particular asperities remain as peak points after the rotation, that is, no distortion. In our experiments, the assumption is justified considering that the tilt angles were $\theta \leq 5.7°$ with $\sin\theta < 0.1$ and $\cos\theta > 0.995$. According to eq 6c, the feature distortion associated with the digital rotation is also negligible.

Figure 7 presents the measured pull-off force against this maximum peak height, excluding the points with rather large positive or negative tilt angles. The figure shows that the pull-off force decreases with the increase of the sample−probe separation approximated by h_{m-s}. This trend is consistent with eq 4. The correlation shown in Figure 7 explains the scattering of the pull-off force measurements caused by titling the sample. In the cases of large positive or negative tilt angles, the highest peaks may be outside the zone that was scanned to generate the topography for the no-tilt case. In addition, the nominal spherical shape may

(29) Mingins, J.; Scheludko, A. *J. Chem. Soc., Faraday Trans.* **1979**, *1*, 75, 1−6.

(30) Bauer, J.; Drescher, G.; Illig, M. *J. Vac. Sci. Technol., B* **1996**, *14*, 2485−2492.

(31) Johnson, K. L. *Contact Mechanics*; Cambridge University Press: Cambridge, 1985.

(32) Ji, Z.; Warzywoda, J.; Sacco, A., Jr. *Microporous Mesoporous Mater.* **2005**, *81*, 1−10.

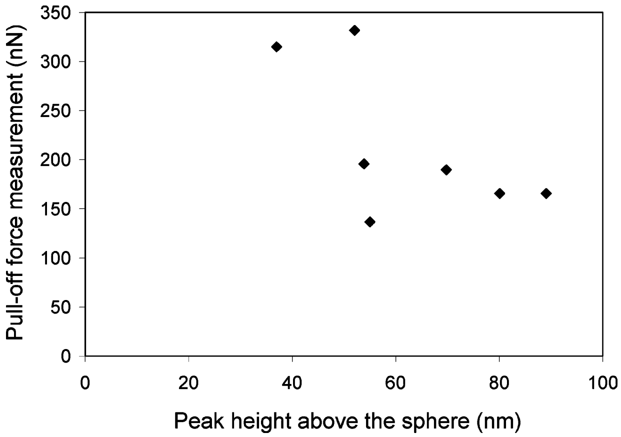

Figure 7. Measured pull-off force vs height of the highest peak above the baseline h_{m-s} at different tilt angles.

also change due to the tilt as the region of the probe that approaches the sample changes. Although the corresponding differences in the radius and center coordinates may be small, they may lead to a significant change in h_{m-s}. As a consequence, the meniscus and the pull-off force seem unpredictable from one tilt angle to another. In understanding the effects of topography on adhesion at the microscale, both the nanoroughness and the micro form of the surface need to be considered.

4. Conclusions

We have measured the pull-off force between a colloidal probe and a silicon sample mounted on wedges at different tilt angles in an environment of controlled relative humidity. The results show that the measured pull-off forces, mainly from the capillary force, are very sensitive to the tilt angle. Detailed examination of the topography by using a direct scanning method and magnitude analysis of the capillary force showed that a continuous meniscus is most likely formed between the probe and the sample. The gap or separation between the two surfaces might be controlled by the maximum height of the probe surface above the highest point of the nominal sphere. This parameter should thus be critical for studying capillary force-dominated adhesion with the colloidal probe technique. Through rotation of the digital image obtained from the direct scanning, the value of this parameter was determined for each tilt angle and its correlation with the measured pull-off force was found to be consistent with the classical capillary force theory. The geometrical parameter depends on the nanoscale surface peak on the probe closest to the sample and the microscale shape of the zone adjacent to the peak. In conclusion, the explicit sensitivity of the measured pull-off force to the tilt angle may be caused by the accompanying change of the contact topography of the colloidal probe. Moreover, the effects of the contact geometry on microscale adhesion are controlled by two important topographic factors: the nanoscale roughness within the contact and the microscale geometry around the contact zone. An accurate characterization of these two factors is therefore a prerequisite to understand and control adhesion in microdevice components. This perspective may also be applied to the study of other microscale contact problems.

Acknowledgment. The authors acknowledge the help of Dr. Purushotham P. Kavuri from the Precision Engineering Division, Manufacturing Engineering Laboratory, at NIST for preparing the SEM images of the colloidal probes. The authors thank Prof. Jan V. Sengers of the University of Maryland and Dr. Gheorghe Stan from the Ceramics Division, Materials Engineering and Science Laboratory, at NIST for their comments on this manuscript.

LA701900F